

Chemical Science

Accepted Manuscript



This is an *Accepted Manuscript*, which has been through the Royal Society of Chemistry peer review process and has been accepted for publication.

Accepted Manuscripts are published online shortly after acceptance, before technical editing, formatting and proof reading. Using this free service, authors can make their results available to the community, in citable form, before we publish the edited article. We will replace this *Accepted Manuscript* with the edited and formatted *Advance Article* as soon as it is available.

You can find more information about *Accepted Manuscripts* in the [Information for Authors](#).

Please note that technical editing may introduce minor changes to the text and/or graphics, which may alter content. The journal's standard [Terms & Conditions](#) and the [Ethical guidelines](#) still apply. In no event shall the Royal Society of Chemistry be held responsible for any errors or omissions in this *Accepted Manuscript* or any consequences arising from the use of any information it contains.

Modulation of Slow Magnetic Relaxation by Tuning Magnetic Exchange in {Cr^{III}Dy^{III}} Single Molecule Magnets†

Stuart K. Langley,^a Daniel P. Wielechowski,^a Veacheslav Vieru,^b Nicholas F. Chilton,^c Boujemaa Moubaraki,^a Liviu F. Chibotaru,^{*,b} and Keith S. Murray^{*,a}

^a*School of Chemistry, Monash University, Clayton, Victoria 3800, Australia. E-mail: keith.murray@monash.edu*

^b*Theory of Nanomaterials Group and INPAC - Institute of Nanoscale Physics and Chemistry, Katholieke Universiteit Leuven, Celestijnenlaan 200F, 3001 Heverlee, Belgium. E-mail: Liviu.Chibotaru@chem.kuleuven.be*

^c*School of Chemistry, The University of Manchester, Manchester M13 9PL, U.K.*

A new series of heterometallic 3d-4f single molecule magnets (SMMs) of general formula [Cr^{III}₂Dy^{III}₂(OMe)₂(RN{(CH₂)₂OH})₂(acac)₄(NO₃)₂] (R = Me, Et, nBu) is reported, displaying slow relaxation of the magnetization and magnetic hysteresis with non-zero coercive fields. Dynamic magnetic susceptibility experiments show that the three complexes possess anisotropy barriers of 34, 37 and 41 K (24, 29 and 26 cm⁻¹); of similar magnitude to their {Co^{III}₂Dy^{III}₂} counterparts. The replacement of the diamagnetic Co^{III} for paramagnetic Cr^{III} ions results in significantly longer relaxation times, as observed via *M(H)* hysteresis at low temperatures, absent for the Co^{III} complexes. The present complexes are also compared to those of a similar Cr^{III}-Dy^{III} complex of formula [Cr^{III}₂Dy^{III}₂(OMe)₂(O₂CPh)₄(mdea)₂(NO₃)₂] (mdeaH₂ = N-methyldiethanolamine), which displays SMM behaviour with a larger anisotropy barrier of 77 K (~54 cm⁻¹) and even longer relaxation times. We show that the long relaxation times compared to the Co^{III} analogues are due to the significant magnetic exchange interactions between the Cr^{III} and Dy^{III} ions, resulting in the suppression of quantum tunnelling of the magnetization (QTM) and leading to a multilevel relaxation barrier. The height of the relaxation barrier in these Cr^{III} systems is then shown to be directly related to the strength of the exchange interactions between the Cr^{III} and Dy^{III} ions, showing a clear route towards enhancing the slow magnetic relaxation of coupled Cr^{III}-Dy^{III} systems.

Introduction

Single-molecule magnets (SMMs) are molecular complexes that possess an energy barrier (U_{eff}) to the inversion of the magnetic moment, resulting in slow relaxation of the magnetization below a blocking temperature (T_B).¹ These complexes are primarily isolated as discrete transition metal (TM)² or lanthanoid³ coordination complexes or as a combination of both.⁴ Understanding the relaxation dynamics in lanthanoid SMM complexes has quickly come to the forefront as it was found such systems revealed intriguing slow magnetic relaxation behavior.⁵ Observations such as extremely large anisotropy barriers have become commonplace for both mono- and polynuclear complexes. Two such examples; {Tb-bisphthalocyaninato}⁶ and {K₂Dy₄}⁷ complexes display values as high as 928 and 692 K for mono- and polynuclear examples, respectively, significantly larger than TM-only compounds.⁸ It has also been noted, however, that a major drawback in such systems is efficient quantum tunnelling of the magnetisation (QTM) at zero magnetic field, where open $M(H)$ hysteresis loops are uncommon. In the cases where hysteresis loops are observed, only very small coercive fields are usually recorded.^{7,9} Recently, exceptions to this have been reported in a small number of radical-bridged Ln^{III} dinuclear compounds; such complexes show strong magnetic exchange between the radical and the Ln^{III} ions and display record hysteresis temperatures for SMMs, of up to $T_B \approx 14$ K, with wide coercive fields.¹⁰ It is believed that the strong magnetic interaction reduces the probability of resonant QTM and significantly increases the relaxation time.^{10a} While these results are very encouraging, it is notable that these types of radical bridged Ln^{III} systems are unique in the literature.

We have therefore adopted a different line of research by promoting strong magnetic exchange via the introduction of 3d transition metal ions incorporated within 4f systems. The recent isolation of a single molecule magnet [Cr^{III}₂Dy^{III}₂(OMe)₂(O₂CPh)₄(mdea)₂(NO₃)₂] (**1**) provided significant validation towards this goal.¹¹ Compound **1** was targeted after our investigation of the planar butterfly {Co^{III}₂Dy^{III}₂} SMM analogue which utilized the diamagnetic Co^{III} ion.¹² This core structure allowed the insertion of the paramagnetic Cr^{III} d³ ion into a simple tetranuclear core, thus switching on magnetic exchange interactions and allowing us to probe what effect the paramagnetic ion had on the magnetic relaxation. Significant Cr^{III}-Dy^{III} exchange interactions were indeed found (J values between -16 and -20 cm⁻¹, ($-J \mathbf{S}_1 \cdot \mathbf{S}_2$ Hamiltonian)) and, pleasingly, the relaxation times became long enough to observe $M(H)$ hysteresis using a conventional SQUID magnetometer, with wide coercive fields, $H_c \approx 2.7$ T, observed at 1.8 K. The use of Cr^{III} is more often than not overlooked

because of its isotropic nature however it can invoke a strong 3d-4f interaction which directly leads to the large coercivity. In an extension of this work, we have synthesised a new series of Cr^{III}-Dy^{III} heterometallic butterfly complexes of formulae [Cr^{III}₂Dy^{III}₂(OMe)₂(mdea)₂(acac)₄(NO₃)₂] (**3**), [Cr^{III}₂Dy^{III}₂(OMe)₂(edea)₂(acac)₄(NO₃)₂] (**4**) and [Cr^{III}₂Dy^{III}₂(OMe)₂(bdea)₂(acac)₄(NO₃)₂] (**5**) (acacH = acetylacetonate, mdeaH₂ = N-methyldiethanolamine, edeaH₂ = ethyldiethanolamine and bdeaH₂ = n-N-butyl-diethanolamine), all of which display SMM behaviour. Complexes **3** – **5** differ from each other by variation of the amine based poly-alcohol ligand. These are, again, analogous to our previously reported Co^{III} containing compounds of general formula [Co^{III}₂Dy^{III}₂(OMe)₂(RN{(CH₂)₂OH}₂)₂(acac)₄(NO₃)₂] (R = (CH₂)₂OH or CH₃) (**2**)¹³ and therefore can be used to study the effect of the paramagnetic spin center. Through comparisons to **1**, the influence of the exchange interaction and the coordination environment around the Dy^{III} ions on the observed barrier height and relaxation times, are now examined. We report the synthesis, structural and magnetic characterization of these three new Cr^{III}-Dy^{III} complexes, together with extensive *ab-initio* and DFT calculations, the theoretical analysis used to determine the factors that govern the slow relaxation behaviour.

Experimental Section

General Information

All reactions were carried out under aerobic conditions. Chemicals and solvents were obtained from commercial sources and used without further purification. Elemental analyses (CHN) were carried out by Campbell Microanalytical Laboratory, University of Otago, Dunedin, New Zealand.

Synthesis of [Cr^{III}₂Dy^{III}₂(OMe)₂(mdea)₂(acac)₄(NO₃)₂] (3**).** CrCl₃·6H₂O (0.13 g, 0.5 mmol) and Dy(NO₃)₃·6H₂O (0.22 g, 0.5 mmol) were dissolved in MeCN (20 mL), followed by the addition of N-methyldiethanolamine (0.06 mL, 0.5 mmol), acetylacetonate (0.1 mL, 1.0 mmol) and triethylamine (0.28 mL, 2.0 mmol), which resulted in a green/blue solution. This solution quickly turned deep purple upon heating and was stirred for 2 hours after which time the solvent was removed to give a purple oil. This was re-dissolved in MeOH and layered with diethylether (Et₂O). Within 5 - 7 days red/pink crystals of **3** had appeared, in approximate

yield of 42 % (crystalline product). Anal. Calculated (found) for **3**: Cr₂Dy₂C₃₂H₅₆O₂₀N₄: C, 30.90 (30.99); H, 4.62 (4.67); N, 4.49 (4.59).

Synthesis of [Cr^{III}₂Dy^{III}₂(OMe)₂(edea)₂(acac)₄(NO₃)₂] (4). The synthesis used for **3** was followed but N-ethyldiethanolamine (0.07 mL, 0.5 mmol) was used in place of N-methyldiethanolamine. Red/pink crystals of **4** appeared within 5 - 7 days, in approximate yield of 55 % (crystalline product). Anal. Calculated (found) for **4**: Cr₂Dy₂C₃₄H₆₀O₂₀N₄: C, 32.05 (32.20); H, 4.74 (4.82); N, 4.40 (4.52).

Synthesis of [Cr^{III}₂Dy^{III}₂(OMe)₂(bdea)₂(acac)₄(NO₃)₂] (5). The synthesis for **3** was again followed but n-N-butyldiethanolamine (0.08 mL, 0.5 mmol) was used in place of N-methyldiethanolamine. Red/pink crystals of **5** appeared within 5 - 7 days, in approximate yield of 32 % (crystalline product). Anal. Calculated (found) for **5**: Cr₂Dy₂C₃₈H₆₈O₂₀N₄: C, 34.31 (34.50); H, 5.15 (5.12); N, 4.21 (4.34).

X-ray crystallography

X-ray measurements for **3** - **5** were performed using a Bruker Smart Apex X8 diffractometer with Mo K α radiation. The data collection and integration were performed within SMART and SAINT+ software programs, and corrected for absorption using the Bruker SADABS program. Compounds **3** - **5** were all solved by direct methods (SHELXS-97), and refined (SHELXL-97) by full least matrix least-squares on all F^2 data.¹⁴ Crystallographic data and refinement parameters for **3** - **5** are summarized in Table 1. Crystallographic details are available in the Supporting Information (SI) in CIF format. CCDC numbers 999241-999243. These data can be obtained free of charge from the Cambridge Crystallographic Data Center via www.ccdc.cam.ac.uk/data_request/cif.

Table 1 Crystallographic data for compounds **3** - **5**.

	3	4	5
Formula ^a	Cr ₂ Dy ₂ C ₃₂ H ₅₆ O ₂₀ N ₄	Cr ₂ Dy ₂ C ₃₄ H ₆₀ O ₂₀ N ₄	Cr ₂ Dy ₂ C ₃₈ H ₆₈ O ₂₀ N ₄
M, g mol ⁻¹	1245.81	1273.86	1329.96
Crystal system	Triclinic	Triclinic	Triclinic
Space group	<i>P</i> -1	<i>P</i> -1	<i>P</i> -1
<i>a</i> /Å	8.7421(3)	10.3553(4)	10.0326(3)
<i>b</i> /Å	12.1359(4)	11.1635(4)	10.7728(3)
<i>c</i> /Å	12.4233(4)	11.1708(5)	11.8721(4)
α /deg	115.5880(10)	67.513(2)	87.039(2)
β /deg	100.6700(10)	83.219(2)	84.943(2)
γ /deg	101.5840(10)	73.283(2)	72.832(2)
V/Å ³	1108.04(6)	1142.70(8)	1220.74(6)
T/K	123(2)	123(2)	123(2)

Z	1	1	1
ρ_{calc} [g cm ⁻³]	1.867	1.851	1.809
λ^{b} /Å	0.71073	0.71073	0.71073
Data Measured	10683	7709	13246
Ind. Reflns	5019	3843	5418
R_{int}	0.0179	0.0197	0.0167
Reflns with $I > 2\sigma(I)$	4651	3558	5105
Parameters	295	286	342
Restraints	0	0	2
R_1^{d} (obs), wR_2^{d} (all)	0.0202, 0.0447	0.0266, 0.0651	0.0207, 0.0501
goodness of fit	1.037	1.080	0.988
Largest residuals/ e Å ⁻³	0.885, -0.500	1.631, -0.530	0.865, -1.386

^a Including solvate molecules. ^b Graphite monochromator.

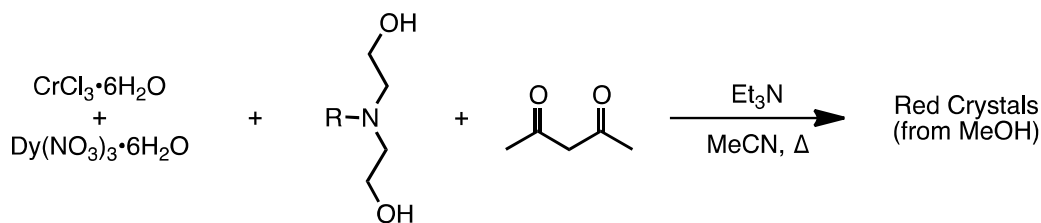
^d $R_1 = \sum ||F_o| - |F_c|| / \sum |F_o|$, $wR_2 = \{ \sum [w(F_o^2 - F_c^2)^2] / \sum [w(F_o^2)^2] \}^{1/2}$.

Magnetic measurements

The magnetic susceptibility measurements were carried out on a Quantum Design SQUID magnetometer MPMS-XL 7 operating between 1.8 and 300 K for dc-applied fields ranging from 0 – 5 T. Microcrystalline samples were dispersed in Vaseline in order to avoid torquing of the crystallites. The sample mulls were contained in a calibrated gelatine capsule held at the centre of a drinking straw that was fixed at the end of the sample rod. Alternating current (ac) susceptibilities were carried out under an oscillating ac field of 3.5 Oe and frequencies ranging from 0.1 to 1500 Hz.

Results and discussion

Scheme 1. Reaction scheme used to isolate compounds **3**, **4** and **5** (R = Me, Et and nBu).



The reaction of the amine-diol and acetylacetonone ligands with the chromium and dysprosium salts resulted in red single crystals being formed (Scheme 1). The single crystals were then exposed to a laboratory X-ray source allowing for structural determinations to be made.

Structural descriptions

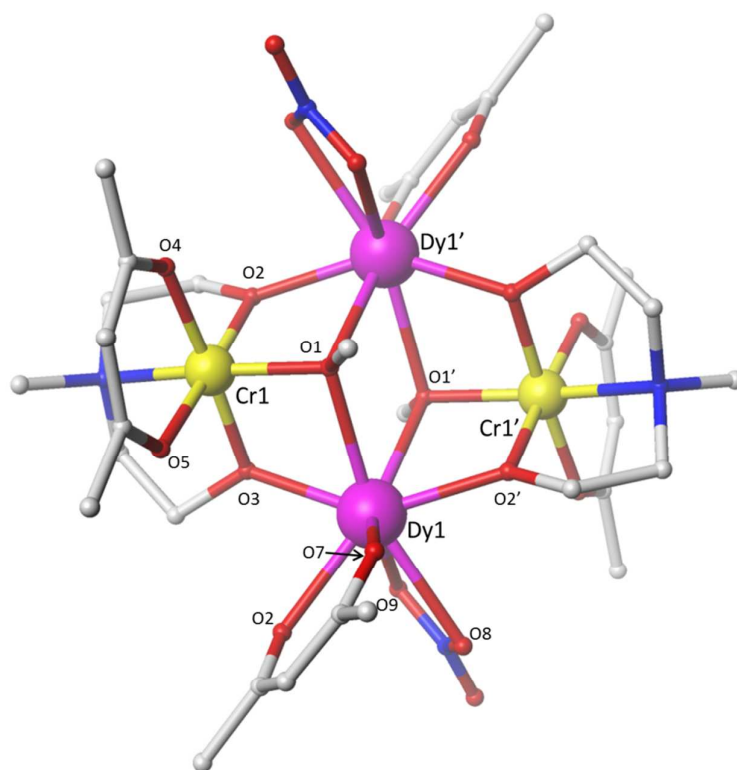


Fig. 1 The molecular structure of compound **3**. The H-atoms are omitted for clarity. Colour scheme; Cr^{III}, yellow; Dy^{III}, purple; O, red; N, blue; C, light grey.

Crystal structure descriptions for [Cr^{III}₂Dy^{III}₂(OMe)₂(mdea)₂(acac)₄(NO₃)₂] (3), [Cr^{III}₂Dy^{III}₂(OMe)₂(edea)₂(acac)₄(NO₃)₂] (4) and [Cr^{III}₂Dy^{III}₂(OMe)₂(bdea)₂(acac)₄(NO₃)₂] (5). Single crystal X-ray diffraction measurements reveal that compounds **3** - **5** crystallize in the triclinic space group *P*-1. Each compound was found to be a heterometallic tetranuclear complex consisting of two Cr^{III} and two Dy^{III} ions, with the asymmetric unit containing half the complex (one Cr^{III} and one Dy^{III} ion) which lies upon an inversion centre. No solvent molecules are found within the crystal. Figure 1 displays the molecular structure of compound **3**, with the structures of **4** and **5** shown in Figures S1 and S2 (ESI). The metallic core arrangements of **3** – **5** are identical, each displaying a butterfly or diamond motif, with the two Dy^{III} ions occupying the ‘body’ positions, with the Cr^{III} ions the outer ‘wing-tip’ sites. The Cr^{III} and Dy^{III} ions are bridged via two μ₃ methoxide ligands, each coordinating two Dy^{III} ions to a single Cr^{III} ion. Each complex is further stabilized around the periphery by two amine-diolate ligands which coordinate via the N-atom to the Cr^{III} ions and then bridge the

Cr^{III} to the Dy^{III} ions via two μ_2 O-atoms. The only chemical difference found between the complexes is the alkyl group associated with the amine-diolate ligands (R = Me (**3**), Et (**4**) and Bu (**5**)). The coordination sphere of each Cr^{III} ion are completed with one chelating [acac]⁻ ligand, while a single chelating [acac]⁻ and a nitrate ligand complete the coordination environment of the Dy^{III} ions. This results in six coordinate Cr^{III} ions with octahedral geometries, displaying an average Cr-L_{N,O} bond distance of 1.98 Å for each complex. The Dy^{III} ions are all eight coordinate with distorted square antiprismatic geometries, with average Dy-O bond lengths of 2.38, 2.37 and 2.38 Å for **3** – **5**, respectively. Selected bond lengths and angles are given in Table 2, using the atom labelling scheme given in Figure 1. Structural comparisons to compound **1** (Figure S3) reveals the absence of a carboxylate bridging pathway between the Dy^{III} and Cr^{III} ions, with two chelating ligands found at the Dy^{III} sites, opposed to one ligand observed for **1**. A single chelating [acac]⁻ is also found at the Cr^{III} sites, not seen for **1**.

Table 2 Selected bond distances (Å) and angles (°) for complexes **3** – **5**.

	3	4	5
Dy1-O7	2.2482(18)	2.268(3)	2.2644(19)
Dy1-O2'	2.2525(15) ^I	2.253(3) ^{II}	2.2448(16) ^{III}
Dy1-O3	2.2642(15)	2.251(3)	2.2646(16)
Dy1-O6	2.3081(18)	2.316(3)	2.3066(18)
Dy1-O9	2.4139(18)	2.436(3)	2.400(2)
Dy1-O1	2.4735(15)	2.457(3)	2.4478(17)
Dy1-O8	2.5336(17)	2.487(3)	2.548(2)
Dy1-O1'	2.5620(16) ^I	2.523(3) ^{II}	2.5913(18) ^{III}
Cr1-O2	1.9299(17)	1.925(3)	1.9183(18)
Cr1-O3	1.9383(16)	1.937(3)	1.9406(17)
Cr1-O5	1.9689(17)	1.972(3)	1.962(2)
Cr1-O1	1.9728(15)	1.976(3)	1.9772(17)
Cr1-O4	1.9755(16)	1.970(3)	1.9803(19)

Cr1-N1	2.1027(19)	2.098(3)	2.118(2)
Dy1 ¹ ...Dy1 ²	4.1742(4)	4.1201(7)	4.052(4)
Dy1 ¹ ...Cr1	3.3521(4)	3.3433(7)	3.3467(4)
Dy1 ² ...Cr1	3.4096(4)	3.4002(7)	3.4230(4)
Dy1-O1- Dy1 ²	111.95(6)	111.63(11)	110.93(7)
Dy1-O1- Cr1	97.20(6)	97.30(11)	97.72(7)
Dy1 ² -O1- Cr1	96.64(6)	97.46(11)	96.12(7)

Symmetry transformation: (I) 1 - x, - y, 1 - z; (II) 1 - x, 2 - y, 1 - z; (III) 2 - x, 2 - y, 1 - z.

Magnetic properties

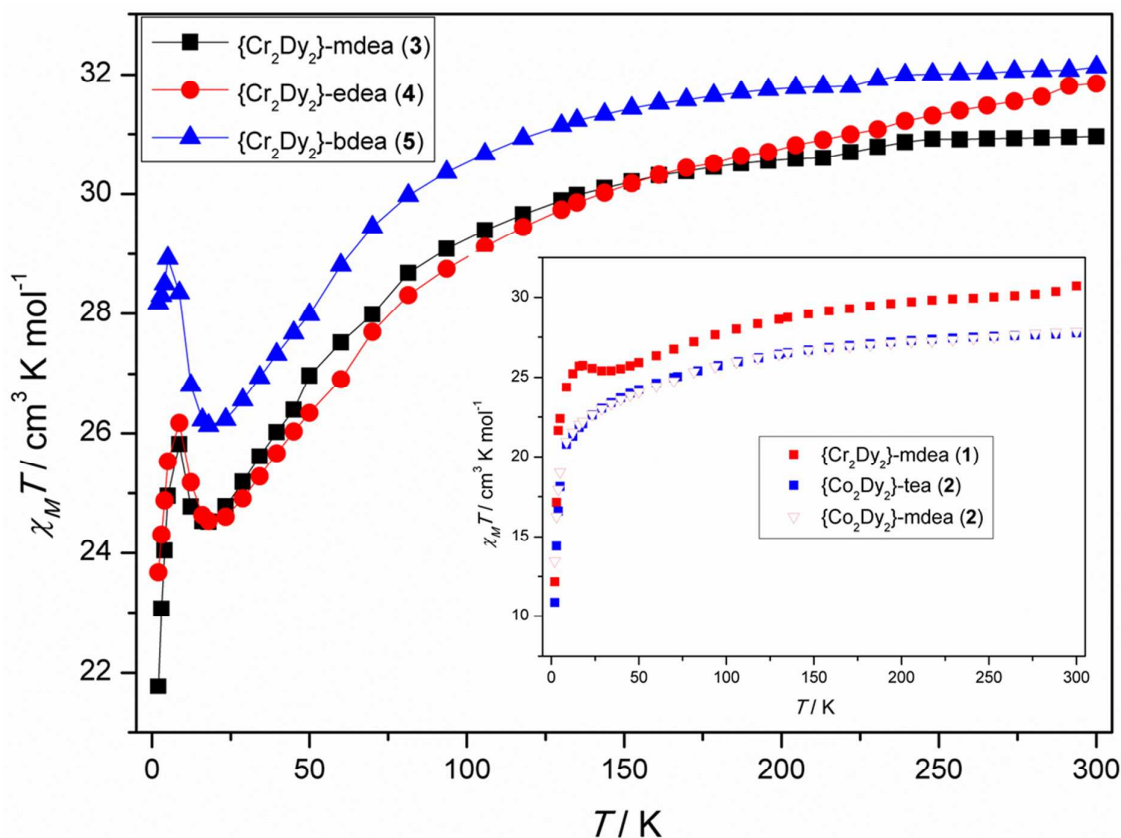


Fig. 2 Variable-temperature dc magnetic susceptibility data for compounds **3** – **5** measured under a 0.1 T applied magnetic field; (inset) dc susceptibility data for **1** and representative examples of the family of compounds denoted as **2**.

In order to probe the magnetic properties, direct current (dc) magnetic susceptibility measurements were performed on polycrystalline samples in the temperature range 2 – 300 K, with an applied magnetic field of 0.1 T. The $\chi_M T$ (χ_M = molar magnetic susceptibility) versus T plots for **3** – **5** (Figure 2), reveal room temperature $\chi_M T$ values of 30.96, 31.85 and 31.19 $\text{cm}^3 \text{K mol}^{-1}$ respectively, which are in good agreement with the value expected for two Cr^{III} ($S = 3/2$, $g = 2$, $C = 1.875 \text{ cm}^3 \text{K mol}^{-1}$) and two Dy^{III} ($S = 5/2$, $L = 5$, ${}^6H_{15/2}$, $g = 4/3$, $C = 14.17 \text{ cm}^3 \text{K mol}^{-1}$) ions that are non-interacting, of 32.09 $\text{cm}^3 \text{K mol}^{-1}$. As the temperature is reduced the $\chi_M T$ value gradually decreases, before a sharper drop occurs between 100 – 25 K, below which an upturn is observed before decreasing again at the lowest temperatures. The high temperature decrease can be attributed to the depopulation of the excited m_J states of the

Dy^{III} ions, while the increase at lower temperatures suggests non-negligible and significant magnetic exchange interactions present between the Dy^{III} and the Cr^{III} ions. The isothermal magnetization (M) measurements for **3** – **5**, plotted as a function of the magnetic field (H), each display a rapid increase in magnetization below 2 T, before following a more gradual linear-like increase, without saturating, thus signifying a significant magnetic anisotropy is present in all complexes (Figures S4 – S6). This is further emphasized by the non-superimposable nature of the reduced magnetization plots (Figures S7 - S9). Compounds **3** - **5** are structurally analogous to the {Co^{III}₂Dy^{III}₂}-acac family **2**, where the Co^{III} ions are diamagnetic and do not contribute to the magnetic behaviour. Plots of $\chi_M T$ versus T for these compounds reveal a continuous decrease in the $\chi_M T$ product upon lowering the temperature (Figure 2, inset), displaying a significantly different temperature dependence to that observed for **3** – **5**. This again suggests that the magnetic interactions between the Cr^{III}-Dy^{III} ions are non-negligible.¹³ The $\chi_M T$ versus T plot of compound **1** is also given in Figure 2, inset and displays a similar temperature dependence to **3** - **5**, however a less pronounced upturn is observed below 25 K indicating a difference in population of the magnetic states and hence exchange strength.

Alternating current (ac) experiments for the {Co^{III}₂Dy^{III}₂}-acac family **2** revealed the presence of slow magnetic relaxation, with anisotropy barriers, U_{eff} in the range 27 - 38 K, with fast quantum tunnelling times of 0.58 – 2.52 ms ($H_{dc} = 0$ Oe).¹¹ We therefore probed compounds **3**, **4** and **5** to determine if any such behaviour is observed, and if so, to attempt to elucidate what role the Cr^{III} ion plays. Variable temperature ac experiments were performed using a 3.5 Oe oscillating ac field with a zero applied dc field, in the frequency range of 0.1 – 1500 Hz. It is found that each complex displays temperature and frequency dependence of both the in-phase (χ_M') and out-of-phase (χ_M'') susceptibility components, confirming the presence of slow relaxation of the magnetization and, thus, SMM behaviour (Figure 3 (**5**) and Figures S10 (**3**) and S11 (**4**)). Compounds **3** – **5** therefore join a small family of Cr^{III}-Dy^{III} complexes which display such behavior.^{11,15}

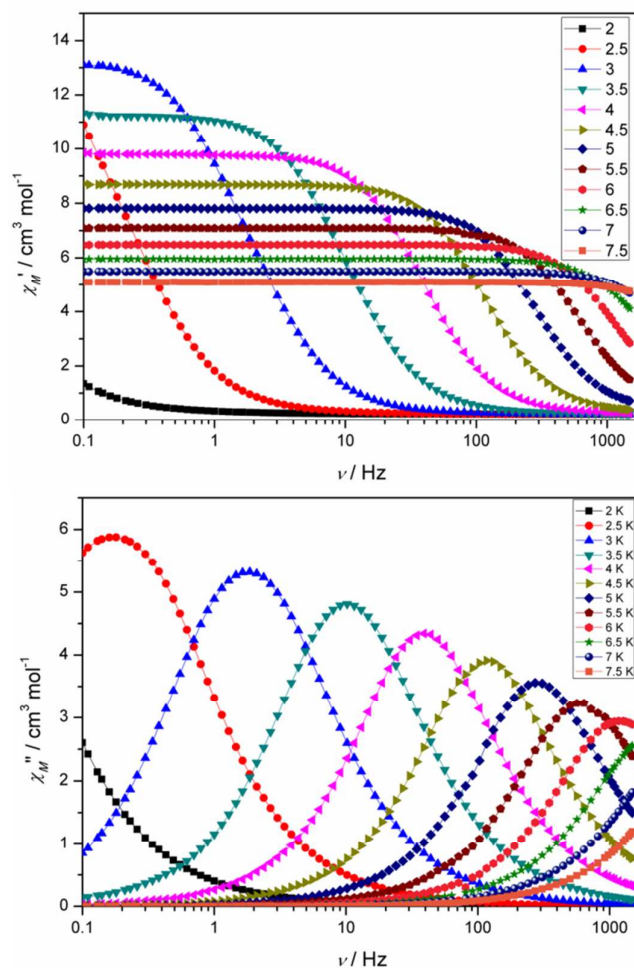


Fig. 3 Isothermal frequency dependence of χ_M' (top) and χ_M'' (bottom) for **5** ($H_{ac} = 3.5$ Oe and $H_{dc} = 0$ Oe).

The $\chi_M''_{\max}$ values were found to be temperature dependent between 2.2 – 4.5 K for **3**, 2.5 – 5.5 K for **4** and 2.5 – 6 K for **5**, over the entire frequency range. This indicates that the relaxation does not cross-over to a pure quantum tunnelling regime on the time-scale of the experiment, contrary to what is observed for the majority of Ln^{III}-based SMMs where QTM is fast (< 1 s).^{13,16} While the experimental evidence indicates that a thermally activated process is dominant, it is found that the $\chi_M''_{\max}$ peak at 2.5 K, while similar for **4** and **5** (0.11 – 0.18 Hz) is shifted to higher frequency for **3** (1.28 Hz). This indicates that the relaxation time at 2.5 K is faster for compound **3** compared to that of **4** and **5**. Cole-Cole plots of χ_M' versus χ_M'' , (Figure 4, inset (**5**) and Figures S12 (**3**) and S13 (**4**), inset) reveal semi-circular profiles thus indicating a single relaxation process is operative. The plots were fitted to a generalized Debye model with α parameters being in the range 0.04 – 0.12, 0.13 – 0.30 and 0.01 – 0.17

for **3**, **4** and **5**, respectively. All α values are small and indicate that there is a very narrow distribution of relaxation times for each complex. It is found that plots of $\ln(\tau)$ versus $1/T$ are linear (Figure 4 (**5**), Figure S12 (**3**) and Figure S13 (**4**)), confirming that a thermally activated Orbach process is operative over the entire temperature and frequency range investigated. Fitting the data to the Arrhenius law [$\tau = \tau_0 \exp(U_{\text{eff}}/k_B T)$] yields anisotropy barriers of 34.6(0.6), 41.6(0.3) and 37.5(0.5) K (24, 29 and 26 cm^{-1}), with $\tau_0 = 1.2 \times 10^{-7}$, 9.2×10^{-8} and 3.1×10^{-7} s for **3**, **4** and **5**, respectively. When the Arrhenius data were extrapolated to low temperatures the relaxation time was found to be 100 s at 1.7 K, 2 K and 1.9 K for **3**, **4** and **5** respectively.

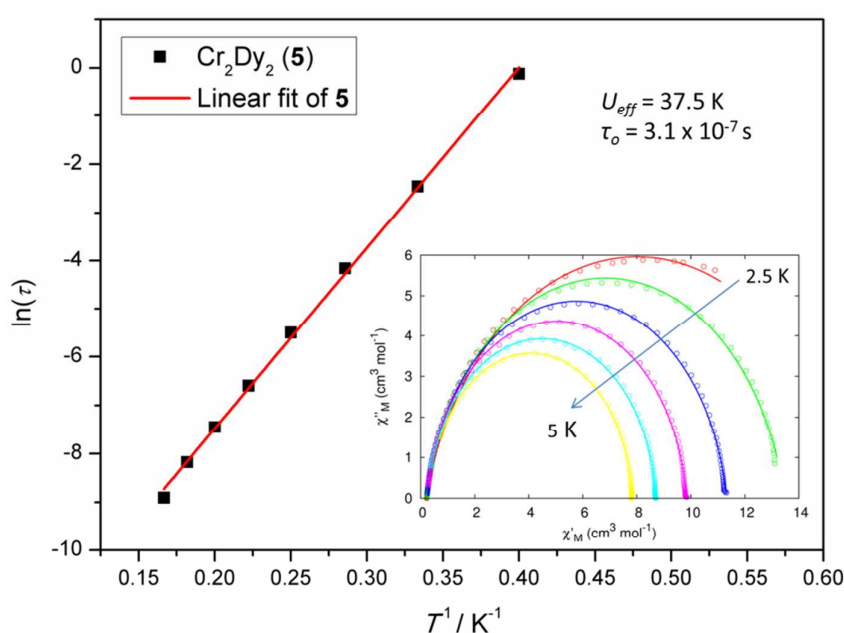


Fig. 4 Magnetization relaxation time (τ) plotted as $\ln(\tau)$ versus T^{-1} for compound **5**. The solid red line represents a fit to the Arrhenius law in the thermally activated regime. (inset) Cole-Cole plots of **5** at temperatures between 2.5 and 5 K. The solid lines are fits of the experimental data using a generalized Debye model.

The effective barrier heights for **3** – **5** are found to be comparable to those of the analogous $\{\text{Co}^{\text{III}}_2\text{Dy}^{\text{III}}_2\}$ complexes, **2**.¹³ The major difference in the relaxation dynamics as determined from the ac data is that the quantum tunnelling is effectively suppressed in **3** – **5**. This is in line with our recent findings for complex **1**, which also has an analogous Co^{III} (diamagnetic ion) counterpart.¹¹ Both displayed similar anisotropy barriers (~ 79 K), the

relaxation mechanism for the $\{\text{Co}^{\text{III}}_2\text{Dy}^{\text{III}}_2\}$ complex crossed over into a pure quantum tunnelling regime below 2.2 K, with a tunnelling time of 0.2 s and no hysteresis loops were observed above 1.8 K. The inclusion of the Cr^{III} ions in the complex resulted in significantly longer relaxation times, with $M(H)$ hysteresis loops observable at temperatures up to 3.7 K, with $H_c \approx 2.7$ T at 1.8 K (sweep rate 0.003 T/s). This was attributed to the suppression of the fast QTM due to the strong magnetic exchange between the Cr^{III} and Dy^{III} ions, which was found to be between -16 and -20 cm^{-1} .¹¹ Furthermore, the anisotropy barrier in **1** was found to follow a relaxation path connecting exchange states of the largest magnetic moments, resulting in a multilevel exchange type path,^{11,17} whereas the majority of Ln based SMMs and in the case of the $\{\text{Co}^{\text{III}}_2\text{Dy}^{\text{III}}_2\}$ complex relax via phonon absorption/emission to a single excited state on individual ions.¹⁸

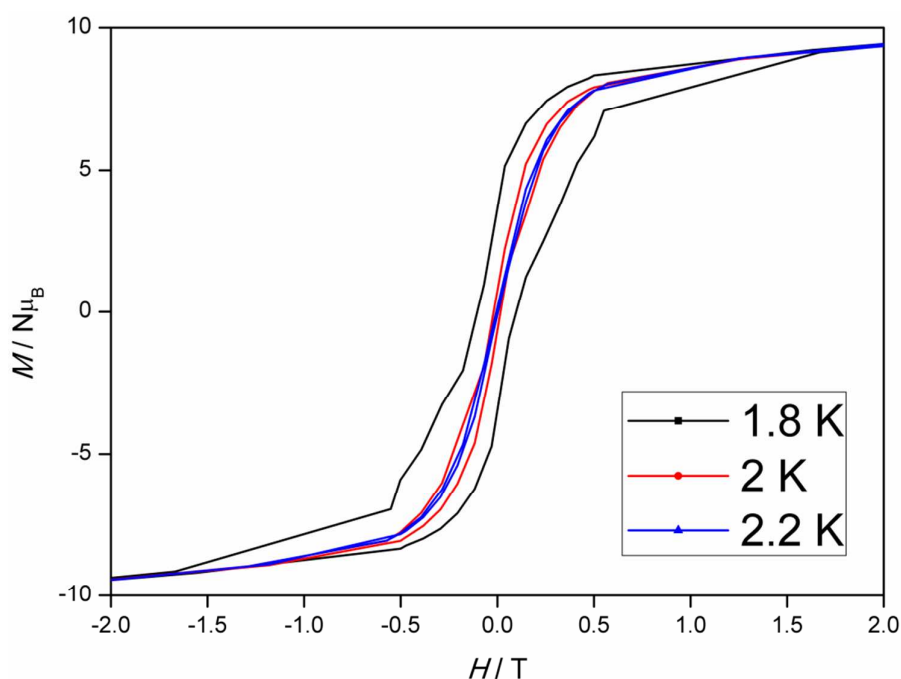


Fig. 5 Plot of magnetization (M) versus field (H) for **5**, sweeping the field with an average sweep rate of 0.004 T/s, at the temperatures indicated.

With compounds **3** – **5** each displaying slow magnetic relaxation on a short timescale (ac data) and because of the appearance of $M(H)$ hysteresis loops for **1**, we also probed to see if **3** – **5** displayed slow magnetic relaxation on a longer timescale. It was found that, again, using sweep rates accessible with a conventional magnetometer, which on average was 0.004 T/s, and with polycrystalline samples, we were able to observe $M(H)$ hysteresis loops at

temperatures up to 1.8 K for **3** (Figure S14) and 2.2 K for **4** (Figure S15) and **5** (Figure 5). The coercive field for **4** and **5** is found to be ~ 1000 Oe at 1.8 K, which decreases with increasing temperature, typical of a SMM. The relaxation times are found to be faster for compound **3**, which displays a very narrow coercive field at 1.8 K, a feature in line with the dynamic behaviour. The appearance of open hysteresis loops unequivocally confirms the magnet like behaviour for **3** - **5**, and, thus, these Cr^{III}-Ln^{III} complexes are rare examples of 3d-Ln SMMs displaying hysteretic behaviour above 1.8 K.^{4a, 4b, 11}

Comparing the experimental magnetic data of **3** - **5**, to those of **1**, we observe significantly different relaxation barriers *viz.* 35 - 41 K ($24 - 29$ cm⁻¹), for **3** - **5**, compared to 77 K (54 cm⁻¹), for **1**, and, as a consequence, faster relaxation times are observed. This is shown via the ac data and the weaker thermal stability of the magnetization as observed in the $M(H)$ hysteresis plots as smaller coercive fields. We do, however, see a significant increase in relaxation times when compared to the analogous Co^{III} containing complexes **2**, which display fast zero field QTM and hence no hysteresis loops are observed above 1.8 K.

Ab initio calculations

To understand the differences just described in the magnetic properties, we have performed *ab-initio* calculations for **3** - **5** using the Molcas 7.8 package.¹⁹ Fragment CASSCF/SO-RASSI/SINGLE_ANISO²⁰ type calculations have been performed to determine the low-lying energy levels and magnetic properties of individual dysprosium centers, whereas the chromium ions were not calculated due to their isotropic nature. Only one dysprosium center per complex has been calculated, due to the presence of the inversion centre. To estimate the values of the exchange coupling constants of the Dy^{III}-Cr^{III}, Cr^{III}-Cr^{III} and Dy^{III}-Dy^{III} pairs, BS-DFT calculations have been employed within the ORCA 3.0.0 program²¹ using the hybrid-type B3LYP functional, which is known to yield good predictions of exchange coupling constants.²² As Dy^{III} ions possess first order orbital angular momentum due to the weak splitting of the 4f orbitals, they generally cannot be described by mono-determinantal methods. Therefore, in all BS-DFT calculations, the Dy^{III} ions were substituted with Gd^{III} ions, which can be described by a single determinant. Indeed, the ground state of the Gd³⁺ ion is a singlet $^8S_{7/2}$, while the first excited state is about 30000 cm⁻¹, meaning that the spin-orbit coupling is operative only in second order perturbation theory. The exchange coupling constants for the isostructural {Cr^{III}₂Gd^{III}₂} complex have been evaluated with Yamaguchi's formula,²³ and the calculated exchange coupling parameter of the Gd^{III}-Cr^{III} pair rescaled to the spin 5/2 of Dy^{III} ion by multiplying the former value by 7/2 and then dividing it by 5/2. In this way we are able to estimate the Lines exchange parameter for the Dy^{III}-Cr^{III} pair.^{11, 24} The

exchange spectrum as well as magnetic properties of the investigated complexes was calculated with the POLY_ANISO program, using the *ab initio* data for the individual Dy^{III} centers obtained in SINGLE_ANISO calculations.^{20d} Detailed information about *ab initio* and DFT calculations is given in the ESI.

The calculated electronic and magnetic properties of the individual Dy^{III} fragments for **3** – **5**, shown in Table 3, reveal the ground Kramers doublets (KDs) of dysprosium ions are well separated from the first excited KDs by ~170 cm⁻¹ and the *g*-tensors are very axial. The low-lying spectrum and the *g*-tensors for compounds **3**, **4** and **5** are very similar, as expected. If we compare these results with those of compound **1**,¹¹ we observe that in the present examples the first excited state is higher in energy by about 70 cm⁻¹, while the *g*-tensor is less axial by an order of magnitude, with *g_x* and *g_y* values for **1** being 0.002 and 0.003, respectively.

Table 3 Energy of low-lying Kramers doublets and the *g*-tensor of the ground KD for **3**, **4** and **5**, with the values extracted for complex **1** shown for comparison.¹¹

3 (cm ⁻¹)	4 (cm ⁻¹)	5 (cm ⁻¹)	1 (cm ⁻¹)
0	0	0	0
169	171	171	101
283	297	317	231
314	328	362	263
367	387	414	308
461	487	509	364
523	559	548	418
700	736	720	703
<i>g_x</i> =0.012 <i>g_y</i> =0.017	<i>g_x</i> =0.014 <i>g_y</i> =0.020	<i>g_x</i> =0.001 <i>g_y</i> =0.016	<i>g_x</i> =0.002 <i>g_y</i> =0.003
<i>g_z</i> =19.70	<i>g_z</i> =19.71	<i>g_z</i> =19.67	<i>g_z</i> =19.82

Given the axiality of the ground KDs for **3** – **5** and the fact that they are well separated from the excited state, we conclude that the exchange interactions should be of the Ising type. Taking into account both the dipolar and exchange interactions, the total Hamiltonian has the following form¹¹:

$$\begin{aligned}
 \hat{H} = & - \left(-J_{dip}^{Dy1-Dy1'} + J_{exch}^{Dy1-Dy1'} \right) \tilde{s}_{Dy1,Z} \tilde{s}_{Dy1',Z} - \left(-J_{dip}^{Cr1-Cr1'} + J_{exch}^{Cr1-Cr1'} \right) \vec{S}_{Cr1} \cdot \vec{S}_{Cr1'} - 3J_{dip}^{Cr-Cr'} S_{Cr1,Z} S_{Cr1',Z} \\
 & - J_{dip}^{Dy1-Cr1} [(1 - 3 \cos^2 \theta) \tilde{s}_{Dy1,Z} S_{Cr1,Z} - 3 \sin \theta \cos \theta \tilde{s}_{Dy1,Z} S_{Cr1,Y}] - J_{dip}^{Dy1'-Cr1'} [(1 - 3 \cos^2 \theta) \tilde{s}_{Dy1',Z} S_{Cr1,Z} + 3 \sin \theta \cos \theta \tilde{s}_{Dy1',Z} S_{Cr1,Y}] \\
 & - J_{dip}^{Dy1-Cr1'} [(1 - 3 \cos^2 \theta) \tilde{s}_{Dy1,Z} S_{Cr1',Z} - 3 \sin \theta \cos \theta \tilde{s}_{Dy1,Z} S_{Cr1',Y}] - J_{dip}^{Dy1'-Cr1'} [(1 - 3 \cos^2 \theta) \tilde{s}_{Dy1',Z} S_{Cr1',Z} + 3 \sin \theta \cos \theta \tilde{s}_{Dy1',Z} S_{Cr1',Y}] \\
 & - J_{exch}^{Dy1-Cr1} \tilde{s}_{Dy1,Z} S_{Cr1,Z} - J_{exch}^{Dy1'-Cr1'} \tilde{s}_{Dy1',Z} S_{Cr1,Z} - J_{exch}^{Dy1-Cr1'} \tilde{s}_{Dy1,Z} S_{Cr1',Z} - J_{exch}^{Dy1'-Cr1'} \tilde{s}_{Dy1',Z} S_{Cr1',Z}
 \end{aligned}$$

where $J_{dip}^{Dy1-Dy1'} = \frac{\mu_B^2 g_{Dy,Z}^2}{R_{Dy1-Dy1'}^3}$; $J_{dip}^{Cr1-Cr1'} = \frac{\mu_B^2 g_{Cr}^2}{R_{Cr1-Cr1'}^3}$; $J_{dip}^{Dy1-Crj} = \frac{\mu_B^2 g_{Dy,Z} g_{Cr}}{R_{Dy1-Crj}^3}$; Eq(1)

Here, the dependence on the θ angle comes from the anisotropy of the dipolar magnetic interaction.

By fitting the magnetic susceptibility data of **3**, **4** and **5** (Figure 6) we derive the exchange coupling parameters (J_{exch}) in Eq.(1) (See Table 4). Notice that all the parameters given in Table 4 correspond to the pseudospin $\tilde{s}=1/2$ of Dy^{III} sites. We see that the exchange interaction between the Dy^{III} and Cr^{III} centers is rather strong, but interestingly it is found to be approximately half the magnitude observed for compound **1**. A possible reason for this difference is that in **1** there are three Dy-O-Cr connecting paths, while in **3** - **5** there are only two.

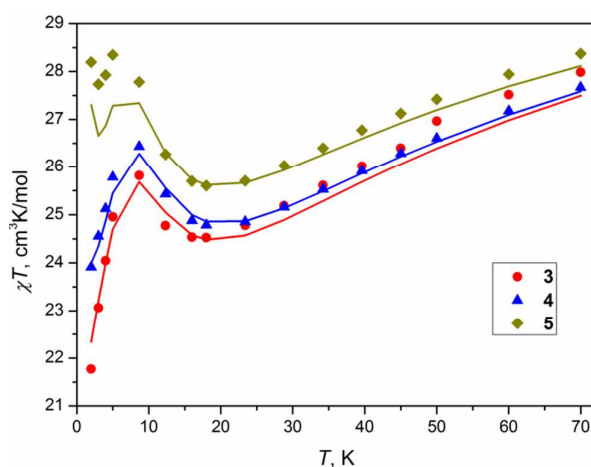


Fig. 6 Plots of $\chi_M T$ versus T for **3** – **5** measured under a 0.1 T magnetic field. Solid lines show the calculated curves. The intermolecular interaction zJ' was 0 cm^{-1} for **4** and set to -0.03 cm^{-1} for **3** and $+0.05\text{ cm}^{-1}$ for **5**. The experimental data of **4** were upscaled with 1% and of **5** downscaled with 2% respectively. No scaling factor was used for **3**.

Further validating the derived exchange coupling parameters from Eq.(1), BS-DFT calculations also predict strong antiferromagnetic interactions between the Dy^{III} and Cr^{III} ions (Table 4), in excellent agreement with the fitted values.²⁵ The only discrepancy found is the sign of the exchange parameter between the Dy^{III} ions in **5**, for which DFT predicts an antiferromagnetic interaction, while the fitted value is ferromagnetic. This is, however, not important due to the relatively small magnitude of this parameter. By analyzing the molecular orbital and the spin density plots (Figures 7, and S16-17) we observe non-negligible tails of

the Cr^{III} and Gd^{III} magnetic orbitals on the same bridging oxygen atoms. Therefore a spin-delocalization mechanism seems to be important, which explains the strong antiferromagnetic Cr^{III}-Dy^{III} interaction. The same reason for the strong exchange interaction was found in **1**.¹¹

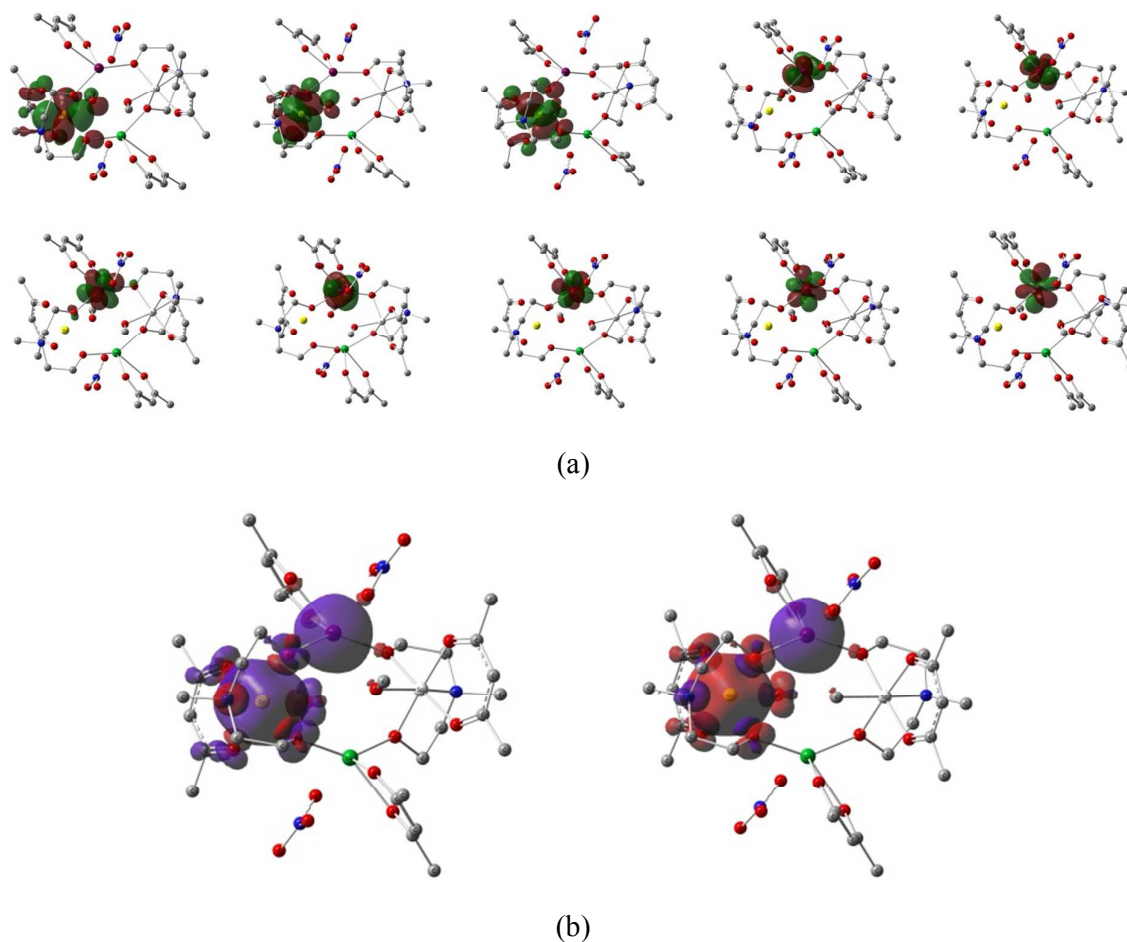


Fig.7 (a) The magnetic orbitals of **3**; (b) Spin density plots of high and low spin configurations, respectively. Blue colour corresponds to spin α and the red one to spin β .

The validity of the DFT-calculated exchange coupling constants is also supported by the calculated magnetization curves, which compare very well with the experimental values (Figure S18-20).

Due to the strong interaction between the Dy^{III} and Cr^{III} ions, the spin of the latter will align along the anisotropy axis of the Dy^{III} ion, antiparallel to its magnetic moment (Figure 8 and S21-22). A similar arrangement of the local magnetic moments occurs in **1**.

Consequently, the Hamiltonian for the low-lying exchange multiplets reduces from Eq.(1) to the following form:

$$\hat{H} = -J_{Dy1-Dy1'}\tilde{s}_{Dy1,z}\tilde{s}_{Dy1',z} - J_{Dy1-Cr1}(\tilde{s}_{Dy1,z}S_{Cr1,z} + \tilde{s}_{Dy1',z}S_{Cr1',z}) - J_{Dy1-Cr1'}(\tilde{s}_{Dy1,z}S_{Cr1',z} + \tilde{s}_{Dy1',z}S_{Cr1,z}) - J_{Cr1,z-Cr1',z}S_{Cr1,z}S_{Cr1',z}$$

Eq (2)

The J constants from Eq.(2) (Table 4) were calculated as combinations of the J_{exch} and J_{dip} parameters by fixing the angles θ in Eq.(1) to the direction shown in Figure 8.

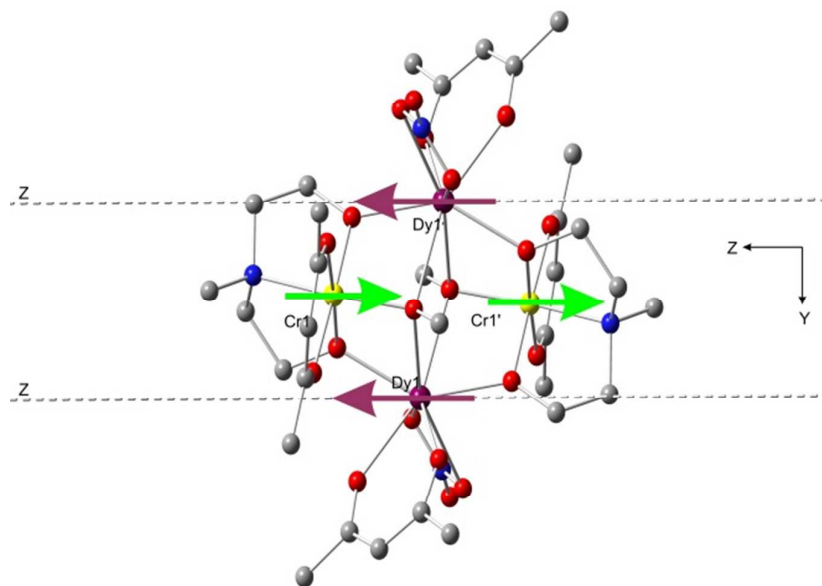


Fig.8 The orientation of local magnetic moments in the ground exchange doublet state in **3**. The dashed lines correspond to the main magnetic axes on Dy^{III} centres.

Table 4 Dipolar and exchange coupling parameters between magnetic centres in **3**, **4** and **5**, with the values extracted for complex **1** shown for comparison.

Complex	3 (cm ⁻¹)				4 (cm ⁻¹)				5 (cm ⁻¹)				
	Calculated		Fitted		Calculated		Fitted		Calculated		Fitted		
Pair	J_{dip}	J_{exch} (BS-DFT)	J_{exch} in Eq(1)	J in Eq(2)	J_{dip}	J_{exch} (BS-DFT)	J_{exch} in Eq(1)	J in Eq(2)	J_{dip}	J_{exch} (BS-DFT)	J_{exch} in Eq(1)	J in Eq(2)	
Dy1-Dy1'	2.31	-0.49	-0.50	-2.64	2.40	-0.49	-0.50	-2.77	2.34	-0.49	0.50	-1.79	
Cr1-Cr1'	0.01	-0.04	-0.04	-0.03	0.01	0.01	0.01	0.02	0.01	0.05	0.05	0.06	
Dy1-Cr1	0.45	-11.27	-11.25	-11.24	0.46	-11.83	-11.85	-11.83	0.45	-10.55	-10.55	-10.48	
Dy1-Cr1'	0.43	-8.35	-8.35	-8.33	0.43	-8.26	-8.25	-7.96	0.42	-7.15	-7.15	-7.14	
1 (cm⁻¹)													
Calculated		Fitted											

J_{dip}	J_{exch} (BS-DFT)	J_{exch} in Eq(1)	J in Eq(2)
2.50	1.00	1.00	-1.50
0.34	0.12	0.10	0.12
5.20	-26.0	-20.50	-20.30
5.20	-32.50	-17.00	-16.70

The obtained spectrum of exchange multiplets together with matrix elements of magnetic moments on the corresponding wave functions can be used for the construction of the barrier of reversal of magnetization following a recently proposed methodology.¹⁷ The barriers thus obtained are of the exchange type since they involve multiple relaxation paths between several exchange levels (Figure 9 A, B and C for **3**, **4** and **5**, respectively). The barriers look similar for all three compounds and they are similar to that for **1** (Figure S23). We would like to stress that the magnetic blocking barriers for **3** and **4** were constructed without using any fitting parameter. The *ab initio* built blocking barriers (ca 23, 24 and 21 cm⁻¹ for **3**, **4** and **5** respectively) are in remarkably good agreement with the experimentally extracted values (24, 29 and 26 cm⁻¹ for **3**, **4** and **5**, respectively). The exchange interaction elucidated in the present compounds is twice as small as in **1** (Table 4), and therefore explains why the experimental magnetization reversal barriers for **3** – **5** are approximately two times lower than in **1** (ca 54 cm⁻¹). This provides strong confirmation that the height of the multi-step relaxation barrier in these systems is related to the strength of the exchange interactions. The discovery that the anisotropy barrier and hence the relaxation mechanism can be controlled by the strength of the exchange interaction is a very important observation. Interestingly, similar experimental findings have been reported for Dy-radical-Dy complexes which, upon replacement of the N₂³⁻ for a bipyrimidinyl radical, resulted in the reduction of the exchange strength and hence a smaller anisotropy barrier was observed, with a weaker thermal dependence in the *M(H)* hysteresis loops.^{10a,c, 27} Observations therefore from the bridged radical work and the present study, clearly show that the anisotropy barrier can be fine-tuned by increasing (or decreasing) the magnetic exchange strength. Simple strategies which may be invoked to effect such changes could involve for example the addition of electron withdrawing/donating groups to the bridging ligands.

It is interesting to note that the coordination environment of the Dy^{III} center(s) which differ significantly between **1** and **3** - **5**, plays only a minor role in influencing the dynamic behavior. This is a consequence of the collective magnetic behavior dominating, as shown by the relationship between the barrier size and the exchange strength. This is contrary to what is

observed for many weakly coupled systems.²⁸ The exchange coupling is therefore more important than the local Dy^{III} geometry as long as the change in local geometry does not drastically alter the $g_z \sim 20$ ground state of the Dy^{III} ion and the exchange pathways are not significantly weakened.

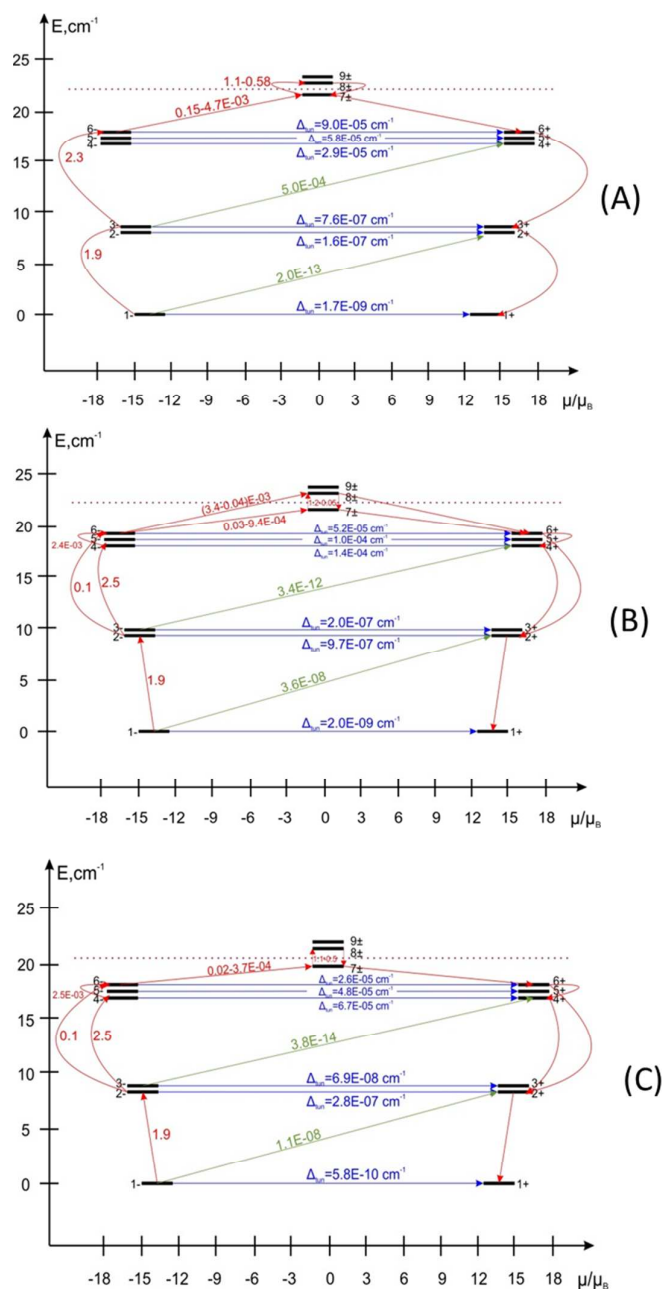


Fig. 9 Low-lying exchange spectrum and the position of the magnetization blocking barrier (dashed pink line) in **3** (A), **4** (B), and **5** (C). The exchange states are placed on the diagram according to their magnetic moments (bold black lines). The

horizontal blue arrows show the tunnelling transitions (the energy splitting) within each doublet state, while the non-horizontal arrows show the spin-phonon transition paths. The numbers at the paths are averaged transition moments in μ_B connecting the corresponding states. Red arrows correspond to the maximal transition probability from a given state, thus outlining the relaxation barrier of reversal of magnetization within the ground exchange doublet.

Conclusions

We have synthesised three new tetranuclear heterometallic Cr^{III}-Dy^{III} single molecule magnets. Direct current magnetic susceptibility measurements reveal significant magnetic interactions occur between the Cr^{III} and Dy^{III} ions in each complex. *Ab-initio* and DFT enabled fits of the data yield 3d-4f exchange parameters between ~ -7 and -12 cm⁻¹; unusually large values for 4f ions, showing that strong exchange can be engineered in conventional metallic clusters. Alternating current susceptibility measurements show that the relaxation is temperature dependent over the entire frequency range, signifying a thermally activated relaxation mechanism, with anisotropy barriers of 34, 37 and 41 K (24, 29 and 26 cm⁻¹) for **3**, **4** and **5**, respectively. Furthermore, magnetic hysteresis is observed up to 2.2 K with a sweep rate of 0.004 T/s. The slow relaxation behavior of **3** – **5** is significantly improved in comparison to the analogous {Co^{III}₂Dy^{III}₂} complex **2** and was shown to be a consequence of strong magnetic exchange resulting in the suppression of the zero-field QTM and the emergence of a multilevel exchange type barrier. A similar multilevel relaxation barrier was reported for the {Cr^{III}₂Dy^{III}₂} complex **1**, however the barrier height found here for **3** – **5** is approximately half the size. It is found that this is due to the weaker magnetic exchange in the present compounds, of approximately half the magnitude as that observed for **1**. Importantly, the results show that the anisotropy barrier can be tailored by modifying the magnetic exchange interaction in complexes containing 4f ions, and as J_{ex} increases, U_{eff} increases, highlighting a clear route towards the enhancement of slow magnetic relaxation of 3d^{III}-4f^{III} coupled systems. Finally, we note that in a recent {Mn^{II}Dy^{III}Mn^{II}} trinuclear Schiff base complex,²⁹ the magnetic relaxation is speeded up rather than slowed down, as occurs in the present complexes; indeed it did not show SMM behaviour whereas the Dy^{III} monomeric analogue did. The Mn^{II}-Dy^{III} exchange in this trinuclear case was weakly ferromagnetic ($J_{Mn-Dy} = 0.22$ cm⁻¹) and, at $T > 2$ K, the weak exchange was believed to act as a fluctuating field at the Dy^{III} centre, thus “quenching” the SMM behaviour. This contrasts markedly with the

present more strongly coupled Cr^{III}-Dy^{III} species. Clearly, there is much scope for exploring other exchange-coupled 3d-4f compounds and studies are underway in our laboratory in this regard.

Acknowledgements

KSM thanks the Australian Research Council (ARC) and the Australia-India Strategic Research Fund (AISRF) for support of this work. VV and LC acknowledge the support of the Flemish Science Foundation (FWO) and of INPAC and Methusalem programs of the University of Leuven. NFC thanks The University of Manchester for a President's Doctoral Scholarship.

†Electronic Supplementary Information (ESI) available: Crystallographic data in CIF format; Figures S1 – S3, molecular structures of **4**, **5** and **1**; Figures S4 to S9, dc magnetic data for **3** - **5**; Figures S10 and S11, ac magnetic data for compounds **3** and **4**; Figures S12 and S13 Arrhenius analysis of the relaxation data and Cole-Cole plots for **3** and **4**; Figures S14 and S15, $M(H)$ hysteresis plots for **3** and **4**; Information regarding *ab-initio* and DFT calculations; Figures S16 and S17, orbital diagrams obtained from DFT calculations; Figures S18 – S20, Fits of the magnetization versus field data; Figures S21 and S22, orientation of local magnetic moments for **4** and **5**; Figure S23, Multi-level magnetization blocking diagram for **1**. See DOI: 10.1039/b000000x/

References

- 1 G. Christou, D. Gatteschi, D. N. Hendrickson and R. Sessoli, *MRS Bull.*, 2000, **25**, 66.
- 2 G. Aromi and E. K. Brechin, *Struct. Bonding*, 2006, **122**, 1.
- 3 (a) D. N. Woodruff, R. E. P. Winpenney and R. A. Layfield, *Chem. Rev.*, 2013, **113**, 5110; (b) P. Zhang, Y.-N. Guo, J. Tang, *Coord. Chem. Rev.*, 2013, **257**, 1728; (c) F. Habib and M. Murugesu, *Chem. Soc. Rev.*, 2013, **42**, 3278.
- 4 For example (a) M. Hołynska, D. Premuzic, I.-R. Jeon, W. Wernsdorfer, R. Clerac and S. Dehnen, *Chem. Eur. J.*, 2011, **17**, 9605; (b) K. C. Mondal, A. Sundt, Y. Lan, G. E. Kostakis, O. Waldmann, L. Ungur, L. F. Chibotaru, C. E. Anson and A. K. Powell, *Angew. Chem. Int. Ed.*, 2012, **51**, 7550; (c) G. Rigaux, R. Inglis, S. Morrison, A. Prescimone, C.

- Cadiou, M. Evangelisti and E. K. Brechin, *Dalton Trans.*, 2011, **40**, 4797; (d) C. Papatriantafyllopoulou, W. Wernsdorfer, A. K. Abboud and G. Christou, *Inorg. Chem.*, 2011, **50**, 421.
- 5 (a) P.-H. Lin, T. J. Burchell, R. Clerac and M. Murugesu, *Angew. Chem. Int. Ed.*, 2008, **47**, 8848; (b) J. Tang, I. Hewitt, N. T. Madhu, G. Chastanet, W. Wernsdorfer, C. E. Anson, C. Benelli, R. Sessoli and A. K. Powell, *Angew. Chem. Int. Ed.*, 2006, **45**, 1729.
- 6 C. R. Ganivet, B. Ballesteros, G. de la Torre, J. M. Clemente-Juan, E. Coronado and T. Torres, *Chem. Eur. J.*, 2013, **19**, 1457.
- 7 R. J. Blagg, L. Ungur, F. Tuna, J. Speak, P. Comar, D. Collison, W. Wernsdorfer, E. J. L. McInnes, L. Chibotaru and R. E. P. Winpenny, *Nature Chem.*, 2013, **5**, 673.
- 8 (a) C. J. Milios, A. Vinslava, W. Wernsdorfer, S. Moggach, S. Parsons, S. P. Perlepes, G. Christou and E. K. Brechin, *J. Am. Chem. Soc.*, 2007, **129**, 2754; (b) J. M. Zadrozny, D. J. Xiao, M. Atanasov, G. J. Long, F. Grandjean, F. Neese and J. R. Long, *Nature Chem.*, 2013, **5**, 577.
- 9 (a) P.-H. Lin, T. J. Burchell, L. Ungur, L. F. Chibotaru, W. Wernsdorfer and M. Murugesu, *Angew. Chem. Int. Ed.*, 2009, **48**, 9489; (b) N. Ishikawa, M. Sugita and W. Wernsdorfer, *J. Am. Chem. Soc.*, 2005, **127**, 3650; (c) J. J. Le Roy, I. Korobkov and M. Murugesu, *Chem. Commun.*, 2014, **50**, 1602.
- 10 (a) J. D. Rhinehart, M. Fang, W. J. Evans and J. R. Long, *J. Am. Chem. Soc.*, 2011, **133**, 14236; (b) J. D. Rhinehart, M. Fang, W. J. Evans and J. R. Long, *Nat. Chem.*, 2011, **3**, 538; (c) S. Demir, J. M. Zadrozny, M. Nippe and J. R. Long, *J. Am. Chem. Soc.*, 2012, **134**, 18546.
- 11 S. K. Langley, D. P. Wielechowski, V. Vieru, N. F. Chilton, B. Moubaraki, B. F. Abrahams, L. F. Chibotaru and K. S. Murray, *Angew. Chem. Int. Ed.*, 2013, **52**, 12014.
- 12 (a) S. K. Langley, N. F. Chilton, L. Ungur, B. Moubaraki, L. F. Chibotaru and K. S. Murray, *Inorg. Chem.*, 2012, **51**, 11873; (b) S. K. Langley, L. Ungur, N. F. Chilton, B. Moubaraki, L.F. Chibotaru and K. S. Murray, *Inorg. Chem.*, 2014, **53**, 4303.
- 13 S. K. Langley, N. F. Chilton, B. Moubaraki and K. S. Murray, *Inorg. Chem.*, 2013, **52**, 7183.
- 14 G. M. Sheldrick, *Acta Cryst. A*, 2008, **A64**, 112.
- 15 (a) J. Rinck, G. Novitchi, W. Van den Heuvel, L. Ungur, Y. Lan, W. Wernsdorfer, C. E. Anson, L. F. Chibotaru and A. K. Powell, *Angew. Chem. Int. Ed.*, 2010, **49**, 7583; (b) H. Xiang, W.-G. Lu, W.-X. Zhang and L. Jiang, *Dalton Trans.*, 2013, **42**, 867; (c) T. Birk, K. S. Pedersen, C. Thuesen, T. Weyhermüller, M. Schau-Magnussen, S. Piligkos, H. Weihe, S. Mossin, M. Evangelisti and J. Bendix, *Inorg. Chem.*, 2012, **51**, 5435; (d) C. Thuesen,

K. S. Pedersen, M. Schau-Magnussen, M. Evangelisti, J. Vibenholt, S. Piligkos, H. Weihe and J. Bendix, *Dalton Trans.*, 2012, **41**, 11284; (e) A. McRobbie, A. R. Sarwar, S. Yeninas, N. Nowell, M. L. Baker, D. Allan, M. Luban, C. A. Muryn, R. G. Pritchard, R. Prozorov, G. A. Timco, F. Tuna, G. F. Whitehead and R. E. P. Winpenny, *Chem. Commun.*, 2011, **47**, 6251.

16 For example (a) P.-E. Car, M. Perfetti, M. Mannini, A. Favre, A. Caneschi and R. Sessoli, *Chem. Commun.*, 2011, **47**, 3751; (b) N. F. Chilton, S. K. Langley, B. Moubaraki, A. Soncini and K. S. Murray, *Chem. Sci.*, 2013, **4**, 1719; (c) P.-H. Lin, T. J. Burchell, R. Clerac and M. Murugesu, *Angew. Chem. Int. Ed.*, 2008, **47**, 8848; (d) S. A. Sulway, R. A. Layfield, F. Tuna, W. Wernsdorfer and R. E. P. Winpenny, *Chem. Commun.*, 2012, **48**, 1508; (e) F. Tuna, C. A. Smith, M. Bodensteiner, L. Ungur, L. F. Chibotaru, E. J. L. McInnes, R. E. P. Winpenny, D. Collison, R. A. Layfield, *Angew. Chem. Int. Ed.* 2012, **51**, 6976; (f) R. A. Layfield, J. J. W. McDouall, S. A. Sulway, D. Collison, F. Tuna, R. E. P. Winpenny, *Chem. Eur. J.* 2010, **16**, 4442.

17 L. Ungur, M. Thewissen, J.-P. Costes, W. Wernsdorfer and L. F. Chibotaru, *Inorg. Chem.*, 2013, **52**, 6328.

18 J. D. Rinehart and J. R. Long, *Chem. Sci.*, 2011, **2**, 2078.

19 F. Aquilante, L. De Vico, N. Ferre, G. Ghigo, P.-A. Malmqvist, P. Neogrady, T. B. Pedersen, M. Pitonak, M. Reiher, B. O. Roos, L. Serrano-Andres, M. Urban, V. Veryazov and R. J. Lindh, *Comput. Chem.*, 2010, **31**, 224.

20 (a) B. O. Roos, P. R. Taylor and P. E. M. Siegbahn. *Chem. Phys.*, 1980, **48**, 157; (b) See the MOLCAS manual: <http://molcas.org/documentation/manual/node95.html>; (c) L. F. Chibotaru and L. Ungur. *Chem. Phys.*, 2012, **137**, 064112; (d) L. F. Chibotaru, L. Ungur, C. Aronica, H. Elmoll, G. Pilet and D. Luneau. *J. Am. Chem. Soc.*, 2008, **130**, 12445.

21 F. Neese, "The ORCA program system" Wiley interdisciplinary Reviews - *Computational Molecular Science*, 2012, Vol 2., Issue 1, Pages 73-78.

22 F. Neese, *Coord. Chem. Rev.*, 2009, **253**, 526.

23 T. Soda, Y. Kitagawa, T. Onishi, Y. Takano, Y. Shigeta, H. Nagao, Y. Yoshioka, K. Yamaguchi, *Chem. Phys. Lett.*, 2000, **319**, 223.

24 M. E. Lines, *J. Chem. Phys.* 1971, **55**, 2977.

25 The relation between the Lines exchange parameters obtained in BS-DFT calculations (J_{Lines}) and those entering in Eq.(1) (J_{exch}) is: $J_{\text{exch}}=25J_{\text{Lines}}$ for Dy-Dy and $J_{\text{exch}}=5J_{\text{Lines}}$ for Dy-

Cr pair.²⁶ For Cr-Cr pair BS-DFT gives the true exchange parameter, i.e., the one entering Eq.(1).

26 L. F. Chibotaru, L. Ungur and A. Soncini. *Angew. Chem. Int. Ed.*, 2008, **47**, 4126.

27 W. W. Lukens, N. Magnani and C. H. Booth, *Inorg. Chem.* 2012, **51**, 10105.

28 (a) S. K. Langley, N. F. Chilton, B. Moubaraki and K. S. Murray, *Chem. Commun.*, 2013, **49**, 6965; (b) F. Habib, G. Brunet, V. Vieru, I. Korobkov, L. F. Chibotaru and M. Murugesu, *J. Am. Chem. Soc.*, 2013, **135**, 13242; (c) J.-L. Liu, Y.-C. Chen, Y.-Z. Zheng, W.-Q. Lin, L. Ungur, W. Wernsdorfer, L. F. Chibotaru and M.-L. Tong, *Chem. Sci.*, 2013, **4**, 3310.

29 A. Bhunia, M. T. Gamer, L. Ungur, L.F. Chibotaru, A. K. Powell, Y. Lan, P. W. Roesky, F. Menges, C. Riehn and G. Niedner-Schatteburg, *Inorg. Chem.* 2012, **51**, 9589.